

Origin and impact of initialisation shocks in coupled atmosphere-ocean forecasts

Article

Accepted Version

Mulholland, D., Laloyaux, P., Haines, K. ORCID:
<https://orcid.org/0000-0003-2768-2374> and Balmaseda, M. A.
(2015) Origin and impact of initialisation shocks in coupled
atmosphere-ocean forecasts. *Monthly Weather Review*, 143
(11). pp. 4631-4644. ISSN 0027-0644 doi:
<https://doi.org/10.1175/MWR-D-15-0076.1> Available at
<https://centaur.reading.ac.uk/40638/>

It is advisable to refer to the publisher's version if you intend to cite from the
work. See [Guidance on citing](#).

Published version at: <http://journals.ametsoc.org/doi/abs/10.1175/MWR-D-15-0076.1>

To link to this article DOI: <http://dx.doi.org/10.1175/MWR-D-15-0076.1>

Publisher: American Meteorological Society

All outputs in CentAUR are protected by Intellectual Property Rights law,
including copyright law. Copyright and IPR is retained by the creators or other
copyright holders. Terms and conditions for use of this material are defined in
the [End User Agreement](#).

www.reading.ac.uk/centaur

CentAUR

Central Archive at the University of Reading

Reading's research outputs online

1 **Origin and impact of initialisation shocks**

2 **in coupled atmosphere-ocean forecasts**

3 David P. Mulholland*

4 *Department of Meteorology, University of Reading, Reading, UK*

5 Patrick Laloyaux

6 *European Centre for Medium-range Weather Forecasts, Shinfield Park, Reading, UK*

7 Keith Haines

8 *Department of Meteorology and National Centre for Earth Observation, University of Reading,*

9 *Reading, UK*

10 Magdalena Alonso Balmaseda

11 *European Centre for Medium-range Weather Forecasts, Shinfield Park, Reading, UK*

12 *Corresponding author address: David Mulholland, Department of Meteorology, University of

13 Reading, Earley Gate, PO Box 243, Reading RG6 6BB, UK

14 E-mail: d.p.mulholland@reading.ac.uk

ABSTRACT

15 Current methods for initialising coupled atmosphere-ocean forecasts often
16 rely on the use of separate atmosphere and ocean analyses, the combination
17 of which can leave the coupled system imbalanced at the beginning of the
18 forecast, potentially accelerating the development of errors. Using a series
19 of experiments with the European Centre for Medium-range Weather Fore-
20 casts coupled system, the magnitude and extent of these so-called initialisa-
21 tion shocks is quantified, and their impact on forecast skill measured. It is
22 found that forecasts initialised by separate ocean and atmospheric analyses
23 do exhibit initialisation shocks in lower atmospheric temperature, when com-
24 pared to forecasts initialised using a coupled data assimilation method. These
25 shocks result in as much as a doubling of root-mean-square error on the first
26 day of the forecast in some regions, and in increases that are sustained for the
27 duration of the 10-day forecasts performed here. However, the impacts of this
28 choice of initialisation on forecast skill, assessed using independent datasets,
29 were found to be negligible, at least over the limited period studied. Larger
30 initialisation shocks are found to follow a change in either the atmospheric or
31 ocean model component between the analysis and forecast phases: changes
32 in the ocean component can lead to sea surface temperature shocks of more
33 than 0.5 K in some equatorial regions during the first day of the forecast. Im-
34 plications for the development of coupled forecast systems, particularly with
35 respect to coupled data assimilation methods, are discussed.

36 **1. Introduction**

37 The use of a coupled atmosphere-ocean model, in preference to an atmosphere-only modelling
38 approach, is essential in order to achieve skillful forecasts of climate on the seasonal timescale and
39 beyond, and is increasingly being recognised to provide benefits at shorter forecast lead times too
40 (e.g., Fu et al. 2007; Klingaman et al. 2008; Vitart et al. 2008; Janssen et al. 2013; Shelly et al.
41 2014). A major challenge of the coupled forecasting approach lies in the initialisation, the goal of
42 which is to incorporate information from the observational network in both atmosphere and ocean
43 into the corresponding model components in an optimal manner. This is commonly achieved
44 through data assimilation (DA), performed using one of a number of established methods for each
45 model component (e.g., Daley 1991; Anderson et al. 1996).

46 The data assimilation strategy used by operational centres in recent years to initialise coupled
47 forecasts (e.g., Saha et al. 2006; Molteni et al. 2011; Arribas et al. 2011; MacLachlan et al. 2014) is
48 to perform separate analyses of the atmosphere and ocean. A sea surface temperature (SST) prod-
49 uct is used to prescribe the boundary condition of the atmospheric model, and the ocean model
50 is constrained by either near-surface atmospheric fields or explicitly specified surface heat, mo-
51 mentum and freshwater fluxes, typically obtained from an atmospheric analysis or from a gridded
52 observational product. One-directional coupling during the initialisation may be achieved with
53 this approach, by using the result of the atmospheric analysis to provide the boundary condition
54 for the ocean model (e.g., Balmaseda et al. 2013). However, the use of different models for the
55 analysis and forecast phases can further complicate matters, particularly when producing histor-
56 ical hindcasts (re-forecasts) for calibration purposes using past initial conditions computed with
57 previous model code versions. In this context, obtaining truly balanced initial conditions requires

58 allowing for some degree of atmosphere-ocean coupling to occur during the analyses themselves,
59 as well as the use of the same coupled model in the analysis and forecast phases.

60 Various possible coupled data assimilation systems exist, exhibiting varying strengths of cou-
61 pling between the atmosphere and ocean. Several operational centres are pursuing such methods
62 (Saha et al. 2010; Lea et al. 2014; Alves et al. 2014), including the European Centre for Medium-
63 range Weather Forecasts (ECMWF) which has developed a prototype for a coupled assimilation
64 system that ingests simultaneously atmospheric and ocean observations (Laloyaux et al. 2015).
65 In this system, information is allowed to cross the interface through the multiple integrations of
66 the coupled model performed during the assimilation process, ensuring a consistent atmosphere-
67 ocean analysis is produced (in the sense that each of the two model components have knowledge
68 about the boundary fluxes of the other component, and have been able to establish a balance with
69 one another in this context). Forecasts can be initialised from the output of this coupled analysis.
70 ECMWF operational coupled forecasts currently, however, continue to use the uncoupled analysis
71 method for initialisation.

72 In choosing an initialisation method, particularly for relatively short-range coupled forecasts,
73 it is important to ensure that the two model components are consistent with one another at the
74 commencement of the forecast, in order to avoid the generation of ‘initialisation shocks’ (alterna-
75 tively, coupling shocks, or spin-up effects) (Rahmstorf 1995; Zhang et al. 2007; Balmaseda et al.
76 2009; Zhang 2011). The likely existence of initialisation shocks in the coupled model context
77 has been acknowledged, particularly in a seasonal forecasting context (Balmaseda and Anderson
78 2009; Marshall et al. 2011), but neither their formation nor impact in short-range forecasts using
79 a full atmosphere-ocean global climate model has been explored in detail, to our knowledge. A
80 particular problem lies in separating out signals of initialisation shock — that is, those that result
81 purely from an imperfect initialisation method — and those of model drift, which occurs regard-

82 less of the initialisation method used, due to the existence of biases, physical or dynamical, in the
83 model (e.g., Magnusson et al. 2013; Wang et al. 2014). Measuring the magnitude of initialisation
84 shock and investigating its causes are important steps in maximising the effectiveness of coupled
85 forecasts and in pointing the way towards possible improvements to conventional methods.

86 Here, we define initialisation shock relatively broadly, to encompass several possible causes,
87 each of which we are able to isolate using the experiments that follow:

88 1. An imbalance, in the vertical fluxes of any of heat, momentum or freshwater, between the
89 atmosphere and ocean initial states, formed due to insufficient communication between the
90 two model components during the calculation of the initial conditions. This situation can arise
91 if model components are coupled to forcing fields other than those of the coupled system
92 during initialisation, such that the near-surface regions of each component are compatible
93 with the relevant forcing fields but will not, in general, be compatible with each other. As a
94 result, when the two components are combined at the beginning of the forecast, rapid changes
95 in surface fluxes are expected, as the two components exchange heat, momentum and/or
96 freshwater in order to establish a new thermodynamical balance. This rapid adjustment could
97 have an undesirable impact on the forecast.

98 2. The use of different models, or different versions or configurations of the same model, to
99 provide the initial state (for either component) and to compute the forecast. A common
100 example of this is the use of a popular reanalysis such as ERA-Interim (Dee et al. 2011) to
101 directly initialise an atmospheric model different to the one used to generate the reanalysis
102 (the reanalysis may then be described as ‘non-native’ with respect to the forecast model). The
103 result could be an initial state that is incompatible with new model’s attractor, resulting in an
104 adjustment at the beginning of the forecast.

105 3. The instantaneous removal of bias correction terms in one of the model components, resulting
106 in an abrupt change in the dynamics of the component at the beginning of the forecast, even
107 in the absence of any model drift (this effect is explained in more detail in Section 3d).

108 This initialisation shock definition is not intended to be a complete list of the contributors to spin-
109 up effects in a model forecast: development of forecast errors due to model biases, in what would
110 be considered ‘standard’ model drift, is *not* included, since this process is unavoidable even with
111 a balanced initialisation using the same models as the forecast itself. Further, model adjustments
112 occurring as a result of the more general problem of assimilating observational information in
113 the initial conditions but not in the forecast itself, are not explicitly considered, as these are also
114 present in all of the forecast systems used in this work. The shocks that are discussed here are
115 those deviations of the forecast from the truth that can demonstrably be reduced or eliminated
116 through changes to the initialisation procedure. Also, we note that a similar initialisation problem
117 exists for the coupling of atmosphere and land surface model components, but do not consider this
118 here: we focus solely on atmosphere-ocean coupling.

119 In this paper, we use the ECMWF analysis and forecast system, in various configurations, to
120 detect the occurrence of initialisation shocks in coupled forecasts; to quantify the contributions
121 to these shocks of each of the mechanisms listed above; and to evaluate the impact of shock on
122 coupled forecasts. By using forecasts initialised using coupled DA as a control, it is possible to
123 isolate those deviations from a reference state that may be described as initialisation shocks, as a
124 subset of the total model drift, which occurs also via the development of systematic model biases.
125 We attempt to establish if effects can be reduced through changes to the initialisation method, and
126 investigate the extent to which the presence of initialisation shocks might affect forecast skill.

127 The structure of the paper is as follows. The models and initialisation techniques used in the
128 paper are introduced, and the experiments performed are defined, in Section 2. The results of these
129 experiments, including identification of initialisation shocks and evaluation of forecast skill, are
130 presented in Section 3. Implications for operational coupled forecasting are discussed in Section 4,
131 and the key findings of the paper are summarised in Section 5.

132 **2. Methods**

133 *a. Models and experiments*

134 The coupled DA system recently developed at ECMWF, called the Coupled ECMWF ReAnal-
135 ysis system (CERA), is presented and described in detail in Laloyaux et al. (2015). The CERA
136 system is based on an incremental variational approach in which the misfits with ocean and atmo-
137 spheric observations are computed by the ECMWF coupled model. Both atmospheric and subsur-
138 face ocean observations are assimilated within a common 24-hour assimilation window, leading to
139 the computation of a coupled atmosphere-ocean analysis. The CERA system uses recent versions
140 of the Integrated Forecast System (IFS), at a spectral resolution of T159 with 137 vertical levels,
141 for the atmosphere, and the Nucleus for European Modelling of the Ocean (NEMO) model, in the
142 ORCA1 configuration (corresponding to a horizontal resolution of around 1° in midlatitudes and
143 $1/3^\circ$ at the equator, with 42 vertical levels) for the ocean (see Table 1 for details of CERA and the
144 other analyses used in this paper).

145 For the purposes of understanding this paper, additional important points to note regarding the
146 CERA system are that SST is nudged towards a gridded observational product during the cou-
147 pled model integrations, rather than being explicitly assimilated, and that bias correction (see
148 Section 3d) is not used in the ocean. The initialisation method used in CERA is presented dia-

149 grammatically in Fig. 1, along with the other approaches to ocean-atmosphere data assimilation
150 that are relevant to this paper. It is intended that the degree of coupling present in the CERA
151 method is sufficient to ensure a consistent initial ocean-atmosphere state, and thus (along with a
152 consistency of models between analysis and forecast) avoid initialisation shocks of the types listed
153 in the previous section.

154 Using CERA, coupled reanalyses were performed covering three two-month test periods (to
155 provide some coverage of the seasonal cycle): Apr–May 2008, Dec–Jan 2008/9 and Aug–Sep
156 2010. 10-day forecasts were initiated at 5-day intervals during these periods, at 00:00 UTC, using
157 the CERA analysis to provide the initial conditions in both the atmosphere and the ocean. This
158 set of 30 forecasts is named C1 (for ‘Coupled’; see Table 2). These forecasts were run with the
159 same model configuration (versions and resolutions) as used in CERA. While the three periods
160 used cover a somewhat limited range (less than 3 years) of the possible background states of the
161 climate system, the consistency of results (shown in the next section) across the three periods gives
162 confidence that our forecast sets are adequate for determining the relative importance of each of
163 the sources of shock.

164 Uncoupled analyses were also performed during these periods. The atmospheric analysis (which
165 is referred to as U_atmos) used the observed SST products as the lower boundary condition, and
166 this analysis was then used as the upper boundary condition during the ocean analysis (referred to
167 as U_ocean), with heat, freshwater and momentum fluxes from U_atmos applied as daily averages
168 (in the same manner as described in Balmaseda et al. (2013)). The same subsurface observations
169 were assimilated, and the same SST nudging scheme was used, as in CERA. A set of forecasts,
170 U1 (for ‘Uncoupled’), with the same resolution as C1, was run using initial conditions obtained
171 from these analyses. We refer to this set as ‘uncoupled’, though in fact a degree of one-directional
172 coupling does exist in the initialisation, through the use of the completed atmospheric analysis

173 during the ocean analysis. Note, also, that the name U1 refers to the uncoupled nature of the
174 analyses only: all forecasts performed here use a coupled system. Comparison of U1 to C1 will
175 reveal the impact on forecasts of the use of coupled DA in creating the initial conditions. With
176 respect to the other experiments detailed subsequently, the key feature of U1 is the use of the same
177 operational ocean and atmosphere models in analyses and forecasts.

178 A third set of forecasts, M1 (for ‘Model change’), was performed, using the same coupled fore-
179 cast model versions as used by C1 and U1. In this set, atmosphere and ocean components were
180 initialised using uncoupled reanalyses, namely ERA-Interim (Dee et al. 2011) for the atmosphere,
181 and ORAS4 (Balmaseda et al. 2013) for the ocean. These reanalyses were performed with the
182 atmospheric and ocean components of the ECMWF coupled forecasting system model, respec-
183 tively (again using a gridded SST product as atmospheric boundary conditions and for ocean SST
184 nudging), but in both cases older, deprecated model versions were used (see Table 1), creating an
185 inconsistency between the analyses and forecasts. In the case of the atmosphere, the resolution
186 between analysis and forecast also differed: ERA-Interim used a resolution of T255 L60, whereas
187 the M1 forecasts were run at T159 L91. In the ocean, analysis and forecast resolutions were the
188 same (ORCA1, 42 vertical levels, as previously). In M1, as in U1, there is some degree of coupling
189 in the initialisation, as ORAS4 was forced by ERA-Interim fluxes during the assimilation.

190 This method, involving older model versions (and possibly lower resolutions) in the creation
191 of initial conditions, is commonly used for the production of historical hindcasts that are needed
192 for the calibration of operational seasonal forecasts (e.g., Arribas et al. 2011), and changes in
193 model version from analysis to forecast may also be a feature of the operational seasonal forecasts
194 themselves (Molteni et al. 2011).

195 Details of all the forecast types are summarised in Table 2. Note that in each case, the initial
196 SST values used are taken from the ocean component of the analysis, rather than the atmospheric

197 component (Fig. 1). In short, the comparison between U1 and C1 is designed to reveal the shock
198 that occurs (in U1) due to atmosphere-ocean imbalance in the initial conditions, while the com-
199 parison between M1 and U1 is aimed at investigating the sensitivity of forecasts to the choice of
200 uncoupled (re)analysis products used for initialisation, i.e. how this choice of initialisation product
201 can generate shocks of the second and third ‘types’, as listed in the previous section. It is expected
202 that any shocks will be detectable within the 10-day range of the forecasts.

203 Two further sets of forecasts are added later (see Section 3d, and Table 2), to distinguish between
204 the second and third sources of shock. Additionally, several 7-month forecasts are performed
205 (see Section 4), to briefly examine the potential for initialisation shocks to impact the forecast on
206 monthly timescales.

207 *b. Forecast evaluation methods*

208 In the results that follow, two common metrics, root-mean-square error (RMSE) and anomaly
209 correlation coefficient (ACC), are used to measure forecast bias and skill respectively. RMSE is
210 sensitive to mean drift so is used to detect shocks and identify absolute-value differences between
211 forecast types. The centred version of ACC, as used here, is insensitive to mean drift (forecast
212 and reference anomalies are calculated with respect to their individual climatologies) so is used
213 to measure forecast skill. For each forecast type, RMSE is calculated with respect to the analysis
214 that was used to initialise that forecast (specifically, CERA for C1, U_atmos and U_ocean for U1,
215 and ERA-Interim and ORAS4 for M1). ACC is calculated for daily mean precipitation, and all
216 forecasts are evaluated against an independent observational dataset (i.e. one not assimilated dur-
217 ing any of the analyses), from the Global Precipitation Climatology Project (GPCP; a daily-mean
218 dataset at 1° spatial resolution) (Huffman et al. 2012), so as to avoid biasing the calculation towards
219 one of forecast types, as would be the case if a particular analysis were used. In the calculation

220 of ACC, forecast and observation ensemble means (averaged over the 30 start dates, at consistent
221 lead times) are used as the climatologies (with respect to which anomalies are computed), since
222 no longer record is available for the forecasts.

223 In several of the figures shown, confidence intervals, with respect to forecast biases or skill being
224 significantly different from the corresponding values in C1, which is taken as a baseline case, are
225 used. These are calculated using a non-parametric bootstrapping approach to account for the finite
226 sample size, (following Goddard et al. 2013; Smith et al. 2013) (details of the procedure are given
227 in the Supplementary Information).

228 **3. Results**

229 *a. Shock in the lower atmosphere*

230 In U1 and M1, the one-way coupling during the assimilation phase is such that continuity from
231 analysis to forecast is provided in the ocean — by virtue of its forcing by the same atmospheric
232 analysis used to provide the initial atmospheric state — but not in the atmosphere. The change in
233 SST forcing experienced by the atmosphere at the beginning of the forecast is the switch from a
234 gridded, observed product to the ocean analysis field, which itself was produced using nudging of
235 SST towards the same observed product (Fig. 1). Therefore, the shock in the near-surface atmo-
236 sphere can be expected to be a function of the accuracy with which the ocean analysis U_ocean
237 reproduces the SST field towards which it has been nudged.

238 Fig. 2(a) shows the root-mean-square difference (RMSD) between the SST seen by the atmo-
239 sphere during analysis (i.e. the gridded observed products) and the SST produced by the ocean
240 analysis U_ocean as initial conditions for the U1 forecasts. Discrepancies are largest in regions
241 of large SST temporal variability, near the northern hemisphere western boundary currents, in the

242 eastern tropical Pacific (particularly during Aug–Sep 2010, when tropical instability waves are
243 most active) and in the Antarctic Circumpolar Current. These are also areas in which model bi-
244 ases, which the assimilation attempts to correct, are large. It is these areas in which shocks due to
245 component imbalance may be expected.

246 Fig. 3 shows the RMSE, after 12 hours, of forecast air temperature at 1000 hPa, for C1 (com-
247 pared to CERA), U1 (compared to U_atmos) and M1 (compared to ERA-Interim), averaged over
248 all forecast start dates. Widespread errors are present in C1 (Fig. 3(a)), forming due to the pres-
249 ence of biases in the models and to any imperfections in the coupled analysis initialisation method.
250 These errors do not constitute the initialisation shock that is being investigated here, according to
251 our earlier definition. Therefore, C1 is taken as a baseline case, such that any further deviation
252 of a forecast from its reference analysis should represent a shock imparted by an initialisation
253 procedure that differs from that of C1.

254 Relative to C1, U1 (Fig. 3(b)) shows, over the ocean, small but significant increases in RMSE in
255 several areas, which are generally those areas in which the RMSE between the two SST fields, as
256 shown in Fig. 2(a), is largest. This air temperature shock signal in U1 therefore appears to develop
257 primarily due to the change in SST forcing felt by the atmosphere after the transition from the
258 analysis to the forecast phase. Correlations between the initial SST discrepancy and the 12 h air
259 temperature error in U1 minus that in C1, calculated across the 30-date forecast set, are significant
260 in the same areas of strong SST variability (Fig. S1(a)), confirming that the development of air
261 temperature biases in excess of those found in C1, can be attributed to the imbalance between
262 atmosphere and ocean at the beginning of the U1 forecasts. These air temperature shocks are
263 generally of magnitude 0.2 K or less, but compared to the small baseline RMSE seen in most areas
264 in C1 (Fig. 3(a)), they represent substantial error amplifications: RMSE is increased by 50% or

265 more in the eastern equatorial Pacific, eastern tropical Atlantic, northern Pacific and across most
266 of the Southern Ocean, and it is more than doubled in the Gulf Stream and Arctic regions.

267 The difference between ORAS4 SST and the gridded products used by ERA-Interim (Fig. 2(b))
268 shows a similar spatial pattern to the differences between the operational analyses, but with slightly
269 larger values (by an average of $\sim 15\%$) in most areas, indicating a greater imbalance and larger
270 discontinuity felt by the atmosphere at the beginning of a forecast. These increases in RMSD are
271 partly the result of small differences between the SST products used by ERA-Interim and ORAS4
272 during two of the three periods covered by these experiments. However, the 1000 hPa air tempera-
273 ture shock in M1 (Fig. 3(c)) is rather different to that in U1: RMSE is increased relative to C1 over
274 most of the ocean, in contrast to the limited areas of amplification seen in U1. Correlations be-
275 tween initial SST discrepancy and 12 h air temperature shock are again significant in some regions
276 (Fig. S1(b)), but are uniformly weaker than those of U1, suggesting the existence of another source
277 of air temperature shock in M1. Also, there is little significant correlation to explain the shocks in
278 parts of the North Pacific, the Southern Ocean near Antarctica and in the Arctic, in which regions
279 (along with most of the globe) the bias is increased several times over its baseline (C1) values.

280 The additional source of atmospheric initialisation shock in M1 is the change in both atmosphere
281 and ocean model versions that occurs between analysis and forecast, combined with the change
282 in atmospheric vertical resolution. The change in atmospheric model is likely to be the more
283 important with respect to shock in the atmosphere, though the change of ocean model could also
284 contribute (as explored further in the next subsection). Model differences lead to a shock that
285 increases errors above those of C1, over most of the planet, by the end of the first day.

286 Fig. 4 compares the RMSE in air temperature throughout the atmospheric column after 24 hours
287 in the forecast types C1, U1 and M1, each evaluated against the analysis used for their initialisa-
288 tion, averaged over the Niño3 region ($150\text{--}90^\circ\text{W}$, $5^\circ\text{N}\text{--}5^\circ\text{S}$). In agreement with the interpretation

289 of the U1 near-surface temperature shock as arising from the initial atmosphere-ocean imbalance,
290 statistically significant differences in RMSE between U1 and C1 are limited to the lower atmo-
291 sphere (at and below ~ 850 hPa). In M1, however, RMSE is amplified compared to C1 at all
292 pressure levels, implying the occurrence of a shock that is spread throughout the atmosphere. This
293 effect might very well arise from the difference in vertical resolution that exists between analysis
294 and forecast (60 and 91 vertical levels respectively), together with differences in physics between
295 the two model versions. Note that the errors at this point in the forecast are generally at least as
296 large as differences between the three analyses.

297 So, although atmospheric initialisation shocks do occur as a result of imbalanced initial condi-
298 tions (i.e. shocks of the first ‘type’ as listed in Section 1), the evidence here suggests that these
299 are smaller than the adjustments that occur following a change in the atmospheric model (shocks
300 of the second type). In the present case the change is merely from an older to a newer version
301 of the same model, and a larger effect can be anticipated if initial conditions are obtained from a
302 structurally different model altogether.

303 Fig. 5 shows the evolution of the air temperature forecast error at 1000 hPa for C1, U1 and
304 M1 against their own analyses, averaged over the Niño3 region. The larger error growth in U1
305 compared to C1 results from the SST discrepancies shown in Fig. 2(a) during the first day, and
306 the effects of the shock are felt out to at least 10 days’ lead time, through a ~ 5 –10% increase
307 in RMSE, showing that initialisation shocks have the potential to impact medium-range (as well
308 as short-range) forecasts. In M1, the effect of the difference in vertical resolution between the
309 forecast and the reference analysis can be seen at lead time $t = 0$, and RMSE rises sharply on day
310 one of the forecast, indicating a strong shock following the change in model version/resolution.
311 Part of the difference between M1 and U1 may be attributable to the lower vertical resolution of

312 M1 (the number of vertical levels in the lowest ~ 1 km is reduced by around a third compared to
313 U1).

314 *b. Shock in the upper ocean*

315 In the upper ocean, markedly different bias development is seen in M1 compared to the other
316 two forecast types, particularly near the equator. Fig. 6 plots the time series in SST averaged in the
317 Niño3 region, for the three forecast types and their corresponding analyses, in the period Dec–Jan
318 2008/9 only. In M1, a large shock occurs at the beginning of the forecast, and a cold bias of around
319 0.5 K has formed after 6 hours, the first output point in the forecast series. A shock of around this
320 size forms consistently ($\pm 20\%$) in each of the 10 forecasts in this period, and the identification
321 of this error is clearly not sensitive to the reference SST used. The other two periods, shown in
322 Fig. S2, feature similar cold shocks, but with different magnitudes. The shock is therefore a robust
323 effect, but shows some seasonal variation, due to seasonal variation in the difference between the
324 climatological states of the analysis and forecast versions of the ocean model. After the initial
325 shock, a correction is seen to occur; nevertheless, by day 10, the M1 error is still significantly
326 larger than errors in the other forecasts. In this case, the initialisation shock has increased the
327 forecast error, though in general the shock need not be of the same sign as the forecast drift (see
328 e.g. Fig. S2(a)). A similar shock, though with smaller magnitude, is seen in the eastern equatorial
329 Atlantic (see Fig. S3).

330 The source of this drift is dynamical differences between the two ocean model versions (as used
331 in ORAS4 and M1 respectively; see Tables 1 and 2), combined with differences in ocean analysis
332 methodology. Upper ocean vertical profiles in the Niño3 region, plotted in Fig. 7, show that the
333 ORAS4 analysis (run with NEMO v3.0) features stronger (by up to 50%) upwelling velocities
334 than CERA and U_ocean at 50 m depth and below. All three analyses are nudged to the same (or

335 a very similar) SST field (analysed Niño3 SSTs show a spread of $\sim 0.2^\circ$ K), and the zonal wind
336 forcings supplied to the ocean analyses (from CERA, U_atmos and ERA-Interim) are very similar
337 (not shown), so differences in upwelling must be due to ocean model differences between the two
338 versions used to perform the analyses, and differences in the treatment of model bias during the
339 analysis (examined further in Section 3d). The shock that occurs in Niño3 in the M1 forecasts
340 does so as a result of the use of the ORAS4 equatorial ocean state as initial conditions in the
341 newer version of NEMO, which normally (in U_ocean, with no bias correction) produces realistic
342 near-surface temperatures with much weaker upwelling. The stronger vertical velocities, as well
343 as colder waters at 50–150 m, while not necessarily less realistic than U_ocean, cause the rapid
344 surface cooling due to their incompatibility with the forecast model. The partial recovery of Niño3
345 SST in Fig. 6 can be interpreted as the equatorial ocean circulation adjusting (weakening) through
346 the use of the newer model version. Differences between the analyses vary seasonally, correlated
347 with the size of the SST shock in M1 in the three forecast periods. A similar explanation can be
348 found for the (weaker) shock that occurs in the eastern equatorial Atlantic.

349 Returning to Fig. 6, it is seen that the drift in C1, which can again be taken as a baseline case, is
350 small in Niño3 in this season, though more substantive drifts do occur in other seasons (Fig. S2).
351 In U1, a cold bias can be seen to form at the beginning of the forecast. However, the source of this
352 bias is not the same as that of the M1 shock. The source is the weak diurnal variation present in
353 SST in the U_ocean analysis, as a result of the use of daily-mean fluxes in its production. Since
354 forecasts are initialised at 00:00 UTC, a longitude-dependent bias forms once the coupled forecast
355 model generates a larger diurnal SST signal. In the eastern Pacific, the initial SST value, which is
356 essentially a daily-mean value, is too cold given the local time of day (seen by comparing the C1
357 and U1 lines at $t = 0$), so, as the region cools in the evening, a bias develops relative to U_ocean.
358 The opposite effect occurs in the Indian Ocean (Fig. S3(b)). C1, on the other hand, does not show

359 this drift, as the CERA ocean analysis includes some diurnal SST variation by virtue of its frequent
360 coupling to the atmosphere during the analysis. The time-of-day effect might be considered to be
361 a legitimate form of shock (in line with the definition given in Section 1), stemming from a lack of
362 coupling during the ocean analysis. However, in principle it is possible to obtain a stronger SST
363 diurnal cycle from an uncoupled ocean analysis by forcing using a higher-frequency atmospheric
364 flux product.

365 Errors introduced due to this effect are of order 0.1 K, and appear to account for most of the
366 U1 drift in this region, which is otherwise not much different to that of C1, implying a limited
367 impact of imbalance-driven shock on SST. Nevertheless, correlations between the SST and air
368 temperature shocks do suggest that part of the U1 SST drift in the eastern Pacific arises due to a
369 compensatory ocean cooling in response to the overlying atmospheric cold shock (Fig. 3(b)).

370 *c. Impact on forecast skill*

371 Having established that initialisation shocks do occur in the upper ocean and in the atmosphere
372 in the forecasts initialised using uncoupled data assimilation, we now investigate whether or not
373 these shocks have any detrimental impact on the forecast skill, using daily average precipitation
374 rates evaluated against GPCP observed rates. The use of an independent reference dataset such as
375 this is the only way to meaningfully compare forecast skill among the different experiments, since
376 each was initialised using a different analysis.

377 Fig. 8 shows that, in both the tropics and extratropics, differences in forecast skill between
378 C1 and U1, which should form solely due to the effects of shock due to initial imbalance, are
379 very small and generally not significant, implying that the impact on forecast skill of this type of
380 initialisation shock is, using this broad measure, slight. Although, where differences in these wide
381 regional averages do briefly reach 90% significance (on two occasions in the northern extratropics)

382 they do so with larger skill scores in C1 than in U1. A similar evaluation of skill in 1000 hPa
383 temperature, measured against an independent reanalysis, also resulted in negligible differences
384 between C1 and U1 (not shown). A much larger forecast set may be necessary to assess confidently
385 the penalty in skill arising from imbalance-driven shock, since it appears to be a very small one,
386 as far as can be determined from this set.

387 The precipitation forecast skill of the M1 forecasts (not shown) is consistently lower, by ~ 0.03 ,
388 than C1 and U1. While this could suggest a sustained impact following the initialisation shock
389 due to the change in model version, it is perhaps more likely to be a symptom of the slightly
390 lower vertical resolution used in M1, and of the less accurate initial atmospheric state provided by
391 ERA-Interim compared to the initial states used in C1 and U1.

392 *d. Sensitivity to ocean initial conditions*

393 Although dynamical differences between the two ocean model versions were seen earlier to
394 explain at least partly the SST shock in M1, there is another difference between the ocean initial-
395 isation methods of M1 and U1 — the use of bias correction during the analysis in M1, and not in
396 U1. Bias correction during the assimilation attempts to prevent the rapid destruction of increments
397 by a biased model, and has an impact on ocean velocities, particularly close to the equator, where
398 model biases tend to be large due to uncertain wind stress forcing of the upper ocean (Bell et al.
399 2004; Balmaseda et al. 2007). The use of bias correction leads ultimately to a different ocean initial
400 state, in the same way as does the use of a different model during analysis. To clarify the reasons
401 for upper ocean shock in M1, a further two sets of forecasts, M2 and M3, were run. Both used
402 ERA-Interim as the atmospheric initial conditions, like M1, and both used the same resolutions as
403 M1, but with different initialisations for the ocean.

404 Forecasts M2 used as initial conditions a different ocean analysis, one identical to ORAS4 but
405 run without bias correction (ORAS4_nobiascrtn; see Balmaseda et al. (2013)). Due to a limited
406 number of available restart files for this analysis, a smaller set of 6 forecast start dates were run
407 in Apr–May 2008 and Dec–Jan 2008/9, and no forecasts were possible in Aug–Sep 2010, so
408 Aug–Sep 2008 was used instead. For all start dates used for M2, corresponding M1 forecasts
409 were also run, enabling an accurate comparison between these two forecast types, to isolate the
410 roles of changing model version and the use of bias correction, in initialisation shocks originating
411 in the ocean. Then, to complete the attribution of shocks to the three sources identified in the
412 introduction, a set of forecasts M3 was run (for the same 30 start dates as in M1) using the new
413 uncoupled ocean analysis (U_ocean) as the ocean initial conditions. The results of M2 should
414 isolate the contribution to the shock in the ocean of the removal of bias correction at the beginning
415 of the forecast, as distinct from the contribution from a change in model version, while M3 should
416 confirm that ocean shocks are predominantly caused by changes in the ocean component between
417 analysis and forecast (and not by changes in the atmospheric component).

418 In M2, the shock at Niño3 (Fig. 9(a)) is only slightly weakened relative to M1 — there is
419 an average reduction of $\sim 25\%$, with little variation across the three seasons — and is virtually
420 unchanged in the eastern Atlantic (Fig. S4(a)). This confirms that the change in ocean model
421 version, rather than the use of bias correction during the analysis, is the dominant cause of these
422 equatorial cold shocks. Subsurface profiles (not shown) show that ORAS4_nobiascrtn upwelling
423 velocities in the Niño3 region are up to 25% weaker than those in ORAS4, explaining the reduced
424 surface cold shock.

425 In other areas, the shock in SST and/or air temperature is slightly increased in M2 relative to M1
426 (see Fig. S4(a) and (b)). Thus, the inclusion of bias correction in the initialising ocean analysis
427 (and its removal during the forecast) imparts small shocks to the upper ocean and to the lower

428 atmosphere (possibly through an increased component imbalance), which can either amplify or
429 reduce the existing shocks following the change in model. In the tropics, the use of bias correction
430 generally has a negative impact on the forecast, as it shifts the ocean analysis circulation into a
431 state that cannot be maintained for any significant length of time from the beginning of the forecast,
432 therefore resulting in an adjustment.

433 In M3, errors in the ocean develop in a similar manner to those of U1, as the two share the same
434 ocean initial conditions. The large M1 shocks at Niño3 (Fig. 9(b)) and in the eastern equatorial
435 Atlantic (see Fig. S4(c)) are entirely absent, confirming that the ocean initialisation is the source
436 of the M1 shocks. The air temperature shock in the eastern Pacific (Fig. S4(d)) is also reduced,
437 relative to M1 — the lack of cold shock in the underlying SST is likely the main reason for this,
438 since the two biases (in SST and 1000 hPa temperature) are strongly correlated in this area in
439 M1. A reduction in atmospheric shock here may arise also due to the slightly better initial balance
440 present in this area in M3 (which is very similar to the balance in U1, shown in Fig. 2(a)) compared
441 to M1. Elsewhere, air temperature RMSE is very similar to that of M1, confirming that it is the
442 change in atmospheric model version that produces a large component of these widespread biases
443 on the first day. The influence of the atmospheric initialisation on SST can be seen in the slightly
444 increased SST drift in M3 compared to U1 (Fig. 9(b)).

445 **4. Discussion**

446 The results presented above suggest a definite impact on short-range forecasts of changes in
447 ocean or atmosphere model between analysis and forecast, but show only a small (though signifi-
448 cant) effect due to an imbalance in the initial conditions. An important factor in the performance
449 of C1 and U1 forecasts is the use of nudging towards a complete gridded SST product, rather than
450 assimilation of individual SST observations, in the ocean analyses. This ensures that U_ocean

451 SSTs remain, almost everywhere, very close to the observational product, the field that is seen by
452 the atmosphere during U_atmos (see Fig. 2(a)). While this is beneficial with regard to minimising
453 initialisation shock in U1, direct assimilation of satellite SST observations may be preferred to
454 nudging in ocean analyses, since the latter is currently done by modifying air-sea fluxes rather
455 than the ocean model itself (Balmaseda et al. 2013). If assimilation is used, any gaps in obser-
456 vational coverage will lead to periods without observational increments during which uncorrected
457 model SSTs could diverge substantially from the field seen by the atmosphere. This would result
458 in imbalances that are more temporally variable, and at times larger, than those shown in Fig. 2.

459 Therefore, the differences in C1 and U1 forecast RMSE and skill shown here should perhaps
460 be taken as a lower limit. That is, the benefits of coupled DA to forecasting may be felt more
461 strongly if assimilation of SST is used rather than nudging in the uncoupled ocean analysis, at
462 least in any data-sparse regions. Where SST nudging is used in conjunction with one-directional
463 coupling of separate ocean and atmosphere analyses, the gains in forecast skill due to reductions in
464 initialisation shock following the implementation of a coupled DA system similar to CERA may,
465 based on these results, be small. This is more a statement of the acceptable degree of balance
466 achieved in the U1 initialisation than a criticism of coupled DA. Additionally, coupled DA may
467 result in a more accurate analysis than uncoupled assimilation (Laloyaux et al. 2015), which could
468 lead to further gains in forecast skill, separate to any achieved through reductions in initialisation
469 shock, although this was not the case in the precipitation results shown here.

470 With regard to the relative merits of a more strongly coupled DA method (one involving the
471 modelling of cross-covariances to spread information between the two model components), while
472 this offers the potential to produce a more balanced initial state than is produced by CERA, which
473 should in itself lead to better forecasts, it seems unlikely that forecast skill will be further improved

474 specifically by a reduction in initialisation shock, judging by the similarity in skill between C1 and
475 U1 (Fig. 8).

476 To mitigate the shocks that can result from the use of bias correction in the ocean analysis
477 (Fig. 9(a)), it can be argued that the bias correction term, estimated during the initialisation phase,
478 should be maintained during the forecast itself. This would not only reduce the overall initialisa-
479 tion shock, but would also slow the model drift. However, this is not possible in forecasts using
480 uncoupled initialisation methods (such as U1, M1 and M2), due to the different biases present in
481 the forced ocean model compared to the coupled forecast model (and potentially differences be-
482 tween the analysis and forecast models themselves). Such a method would be possible in a forecast
483 of type C1, however, and the viability and usefulness of this approach should be investigated.

484 A further consideration, not described so far in this paper, is that large adjustments in the upper
485 ocean (evidence of which was seen in Fig. 6) could generate shock signals that propagate beyond
486 the 10-day duration of the forecasts shown here, due to the longer dynamical timescale of the
487 upper ocean. Several exploratory 7-month forecasts, which are described in the Supplementary
488 Information, have shown evidence of spurious Rossby waves propagating westward in the equato-
489 rial Pacific, following a change in ocean model version between analysis and forecast. Significant
490 differences in the upper ocean between forecasts of type M1 and M3 were seen at lead times of
491 up to 7 months (see Figs. S5 & S6). The impact on seasonal forecasts of using non-native ocean
492 models for initialisation is a possible area for further study.

493 The results of this work should serve as useful guidance for medium-range and seasonal fore-
494 casting at operational centres. Besides finding hints of a slight increase in atmospheric forecast
495 skill when using coupled DA rather than uncoupled assimilation methods for initialisation, we
496 have also shown that initialisation shock can be generated through the use of non-native models
497 for the creation of initial conditions. Depending on the resources available to an operational centre,

498 using initial conditions derived from an older version of the operational forecast model, possibly
499 at lower resolution, or from another model entirely, may be the most practical option for seasonal
500 forecasting. Even if not the case for the forecast itself, this may be more common in performing
501 the set of calibration hindcasts (e.g., MacLachlan et al. 2014) that forms an essential component of
502 a seasonal forecast (and is also valuable at shorter ranges (Hamill et al. 2004)). The hindcasts are
503 used to compute a posteriori bias correction terms, so it is important that the temporal evolution
504 of bias in the hindcasts is as similar as possible to the development of bias in the forecast (as dis-
505 cussed by Hamill et al. 2004). In either case, it has been shown that using non-native analyses for
506 forecast or hindcast initialisation does result in substantial initialisation shocks in both atmosphere
507 and ocean.

508 Various studies have declined to use non-native atmospheric analyses directly as initial condi-
509 tions for coupled forecasts, preferring to nudge towards these analyses (e.g., Hudson et al. 2011)
510 or to initialise a model atmosphere by forcing with observed SSTs (e.g., Alessandri et al. 2010).
511 The results above confirm that there is indeed good reason to avoid direct use of a non-native anal-
512 ysis (even when derived from the same model ‘family’) in initialisation, in the ocean as well as
513 in the atmosphere, if possible. The detrimental aspect of nudging a forecast model towards such
514 an analysis lies in the production of initial conditions that may lie further from the truth, and the
515 optimal nudging strength — one which balances accuracy in the initial state with minimisation of
516 shock, so as to produce the most skilful forecast — is likely to be strongly model dependent. For
517 example, we have not investigated whether or not a forecast system initialised from ERA-Interim
518 and ORAS4, and comprised of model versions 31r2 and 3.0 (see Table 1), outperforms M1 in
519 forecast skill by removing a major component of the initialisation shock at the expense of using
520 deprecated, and inferior, forecast models. The decision over whether or not to use the operational
521 forecast system without also generating initial conditions using the same system will depend on

522 the degree of improvement offered by the newer system in comparison to the one which generated
523 the initial conditions that are already available. Our results do suggest that, where possible, initial
524 conditions for both forecasts and hindcasts should be obtained through analyses using the same
525 models.

526 **5. Conclusions**

527 We have identified initialisation shocks in sets of coupled forecasts for which the initial condi-
528 tions were obtained using uncoupled data assimilation in the atmosphere and ocean. Three distinct
529 sources of shock, with varying degrees of impact on the forecasts, have been identified:

- 530 1. A lack of balance between the atmospheric and oceanic components of the initial state exerts
531 an influence on the forecast drift, as seen through the comparison of forecast types C1 and
532 U1. Initialisation shocks of this type occur most strongly in regions of large SST temporal
533 variability. Their impact on forecast skill, measured by ACC in total precipitation rates,
534 appears to be neutral. This source of shock may be atypically weak in the present case due
535 to the use of SST nudging in the ocean analysis, which limits the size of atmosphere-ocean
536 imbalances that can form in the initial conditions.
- 537 2. A change in model version from analysis to forecast, which occurs in the atmosphere in M3
538 and in both ocean and atmosphere in M1 and M2, leads to larger and more widespread initial-
539 isation shocks. These occur due to differences between model attractors, and are particularly
540 strong in the equatorial ocean, in the present case. Oceanic shocks have the potential to exert
541 an influence on the seasonal timescale.
- 542 3. The use of bias correction during the ocean analysis, and its removal during the forecasts, can
543 impart further initialisation shocks in the upper ocean, at least when different model versions

544 are used for analysis and forecast. These shocks are generally less substantial than those
545 caused by the change in model.

546 These results strengthen the case for operational seasonal forecasting centres to perform new ocean
547 and atmosphere reanalyses, and consistent sets of calibration hindcasts, whenever the operational
548 model is upgraded. The benefit to forecasting of aiming to minimise initialisation shock by using
549 coupled data assimilation to produce these analyses, rather than performing uncoupled assimila-
550 tion using the operational models, is less clear, but may emerge more strongly if assimilation of
551 SST is used in preference to nudging towards a gridded product, during the ocean analysis.

552 *Acknowledgments.* We thank three anonymous reviewers for their comments, which have im-
553 proved the clarity of this manuscript. This work was funded by the UK Natural Environment
554 Research Council (ERGODICS project), the European Space Agency (Data Assimilation Project)
555 and the European Commission (ERA-CLIM2 FP7 project). The work was accomplished through
556 an ECMWF Special Project (spgbhain).

557 **References**

558 Alessandri, A., A. Borrelli, S. Masina, A. Cherchi, S. Gualdi, A. Navarra, P. Di Pietro, and A. F.
559 Carril, 2010: The INGV-CMCC seasonal prediction system: improved ocean initial conditions.
560 *Mon. Weather Rev.*, **138** (7), 2930–2952.

561 Alves, O., Y. Yin, L. Shi, R. Wedd, D. Hudson, P. Okely, and H. Hendon, 2014: A coupled
562 ensemble ocean data assimilation system for seasonal prediction and its comparison with other
563 state-of-the-art systems. *EGU General Assembly Conference Abstracts*, EGU General Assembly
564 Conference Abstracts, Vol. 16, 9487.

565 Anderson, D. L. T., J. Sheinbaum, and K. Haines, 1996: Data assimilation in ocean models. *Rep.*
566 *Prog. Phys.*, **59 (10)**, 1209.

567 Arribas, A., and Coauthors, 2011: The GloSea4 ensemble prediction system for seasonal forecast-
568 ing. *Mon. Weather Rev.*, **139 (6)**, 1891–1910.

569 Balmaseda, M., and D. Anderson, 2009: Impact of initialization strategies and observations on
570 seasonal forecast skill. *Geophys. Res. Lett.*, **36 (1)**.

571 Balmaseda, M. A., D. Dee, A. Vidard, and D. L. T. Anderson, 2007: A multivariate treatment of
572 bias for sequential data assimilation: Application to the tropical oceans. *Q. J. Roy. Meteor. Soc.*,
573 **133 (622)**, 167–179.

574 Balmaseda, M. A., K. Mogensen, and A. T. Weaver, 2013: Evaluation of the ECMWF ocean
575 reanalysis system ORAS4. *Q. J. Roy. Meteor. Soc.*, **139 (674)**, 1132–1161.

576 Balmaseda, M. A., and Coauthors, 2009: Ocean initialization for seasonal forecasts. *Oceanogra-*
577 *phy*, **22 (3)**, 154.

578 Bell, M. J., M. J. Martin, and N. K. Nichols, 2004: Assimilation of data into an ocean model with
579 systematic errors near the equator. *Q. J. Roy. Meteor. Soc.*, **130 (598)**, 873–893.

580 Daley, R., 1991: *Atmospheric data analysis*. Cambridge University Press.

581 Dee, D. P., and Coauthors, 2011: The ERA-Interim reanalysis: Configuration and performance of
582 the data assimilation system. *Q. J. Roy. Meteor. Soc.*, **137 (656)**, 553–597.

583 Fu, X., B. Wang, D. E. Waliser, and L. Tao, 2007: Impact of atmosphere-ocean coupling on the
584 predictability of monsoon intraseasonal oscillations. *J. Atmos. Sci.*, **64 (1)**, 157–174.

- 585 Gemmill, W., B. Katz, and X. Li, 2007: Daily real-time global sea surface temperature — High
586 resolution analysis at NOAA/NCEP. Tech. rep., NOAA/NWS/NCEP/MMAB Office Note Nr.
587 260, 39 pp (available at: <http://polar.ncep.noaa.gov/sst/>).
- 588 Goddard, L., and Coauthors, 2013: A verification framework for interannual-to-decadal predic-
589 tions experiments. *Clim. Dyn.*, **40** (1-2), 245–272.
- 590 Hamill, T. M., J. S. Whitaker, and X. Wei, 2004: Ensemble reforecasting: Improving medium-
591 range forecast skill using retrospective forecasts. *Mon. Weather Rev.*, **132** (6), 1434–1447.
- 592 Hudson, D., O. Alves, H. H. Hendon, and G. Wang, 2011: The impact of atmospheric initialisation
593 on seasonal prediction of tropical pacific SST. *Clim. Dyn.*, **36** (5-6), 1155–1171.
- 594 Huffman, G. J., D. T. Bolvin, and R. F. Adler, 2012: GPCP Version 1.2 1-Degree Daily (1DD)
595 Precipitation Data Set. WDC-A, NCDC, Asheville, NC. NASA/GSFC, Data set accessed June
596 2014 at <http://precip.gsfc.nasa.gov>.
- 597 Janssen, P., and Coauthors, 2013: Air-sea interaction and surface waves. Technical Memorenda
598 712, ECMWF.
- 599 Klingaman, N. P., P. M. Inness, H. Weller, and J. M. Slingo, 2008: The importance of high-
600 frequency sea surface temperature variability to the intraseasonal oscillation of Indian monsoon
601 rainfall. *J. Climate*, **21** (23), 6119–6140.
- 602 Laloyaux, P., M. Balmaseda, D. Dee, K. Mogensen, and P. Janssen, 2015: A coupled data assimi-
603 lation system for climate reanalysis, submitted to *Q. J. Roy. Meteor. Soc.*
- 604 Lea, D., I. Mirouze, M. Martin, A. Hines, C. Guiavarch, and A. Shelly, 2014: The Met Office
605 Coupled Atmosphere/Land/Ocean/Sea-Ice Data Assimilation System. *EGU General Assembly*
606 *Conference Abstracts*, Vol. 16, 12097.

607 MacLachlan, C., and Coauthors, 2014: Global Seasonal Forecast System version 5 (GloSea5): a
608 high resolution seasonal forecast system. *Q. J. Roy. Meteor. Soc.*.

609 Magnusson, L., M. Alonso-Balmaseda, S. Corti, F. Molteni, and T. Stockdale, 2013: Evaluation
610 of forecast strategies for seasonal and decadal forecasts in presence of systematic model errors.
611 *Clim. Dyn.*, **41 (9-10)**, 2393–2409.

612 Marshall, A. G., D. Hudson, M. C. Wheeler, H. H. Hendon, and O. Alves, 2011: Assessing the
613 simulation and prediction of rainfall associated with the MJO in the POAMA seasonal forecast
614 system. *Clim. Dyn.*, **37 (11-12)**, 2129–2141.

615 Molteni, F., and Coauthors, 2011: *The new ECMWF seasonal forecast system (System 4)*. Euro-
616 pean Centre for Medium-Range Weather Forecasts.

617 Rahmstorf, S., 1995: Climate drift in an ocean model coupled to a simple, perfectly matched
618 atmosphere. *Clim. Dyn.*, **11 (8)**, 447–458.

619 Reynolds, R. W., N. A. Rayner, T. M. Smith, D. C. Stokes, and W. Wang, 2002: An improved in
620 situ and satellite SST analysis for climate. *J. Climate*, **15 (13)**, 1609–1625.

621 Saha, S., and Coauthors, 2006: The NCEP climate forecast system. *J. Climate*, **19 (15)**, 3483–
622 3517.

623 Saha, S., and Coauthors, 2010: The NCEP climate forecast system reanalysis. *B. Am. Meteorol.*
624 *Soc.*, **91 (8)**, 1015–1057.

625 Shelly, A., P. Xavier, D. Copsey, T. Johns, J. M. Rodríguez, S. Milton, and N. Klingaman, 2014:
626 Coupled versus uncoupled hindcast simulations of the Madden-Julian Oscillation in the Year of
627 Tropical Convection. *Geophys. Res. Lett.*, **41 (15)**, 5670–5677.

- 628 Smith, D. M., R. Eade, and H. Pohlmann, 2013: A comparison of full-field and anomaly initial-
629 ization for seasonal to decadal climate prediction. *Clim. Dyn.*, **41 (11-12)**, 3325–3338.
- 630 Stark, J. D., C. J. Donlon, M. J. Martin, and M. E. McCulloch, 2007: OSTIA: An operational, high
631 resolution, real time, global sea surface temperature analysis system. *OCEANS 2007-Europe*,
632 IEEE, 1–4.
- 633 Vitart, F., and Coauthors, 2008: The new VAREPS-monthly forecasting system: A first step to-
634 wards seamless prediction. *Q. J. Roy. Meteor. Soc.*, **134 (636)**, 1789–1799.
- 635 Wang, C., L. Zhang, S.-K. Lee, L. Wu, and C. R. Mechoso, 2014: A global perspective on CMIP5
636 climate model biases. *Nature Clim. Change*, **4 (3)**, 201–205.
- 637 Zhang, S., 2011: A study of impacts of coupled model initial shocks and state-parameter optimiza-
638 tion on climate predictions using a simple pycnocline prediction model. *J. Climate*, **24 (23)**,
639 6210–6226.
- 640 Zhang, S., M. J. Harrison, A. Rosati, and A. Wittenberg, 2007: System design and evaluation
641 of coupled ensemble data assimilation for global oceanic climate studies. *Mon. Weather Rev.*,
642 **135 (10)**, 3541–3564.

643 **LIST OF TABLES**

644 **Table 1.** Details of the various analyses (atmosphere, ocean or coupled) that are used
645 for forecast initialisation and as reference fields for forecast evaluation in this
646 paper. The gridded SST product used is either the Operational Sea surface Tem-
647 perature and sea Ice Analysis (OSTIA) (Stark et al. 2007) or one of two Na-
648 tional Centers for Environmental Prediction (NCEP) products (Reynolds et al.
649 2002; Gemmill et al. 2007), depending on the time period (during 2008–2010)
650 in question. The name ‘CERA’ is used to denote both its atmosphere and ocean
651 components. 31

652 **Table 2.** Description of forecast sets described in the text. All forecasts use the same
653 operational coupled ocean-atmosphere model system (model versions 40r1 and
654 3.4 for IFS and NEMO respectively), but types differ in the model versions and
655 settings used for their initialisation (refer to Table 1). The sources of shock
656 considered are the three listed in Section 1. 32

657 TABLE 1. Details of the various analyses (atmosphere, ocean or coupled) that are used for forecast initiali-
658 sation and as reference fields for forecast evaluation in this paper. The gridded SST product used is either the
659 Operational Sea surface Temperature and sea Ice Analysis (OSTIA) (Stark et al. 2007) or one of two National
660 Centers for Environmental Prediction (NCEP) products (Reynolds et al. 2002; Gemmill et al. 2007), depending
661 on the time period (during 2008–2010) in question. The name ‘CERA’ is used to denote both its atmosphere and
662 ocean components.

Name	Atmosphere/ocean	Model version	Resolution	SST treatment
CERA	Atmosphere and ocean	40r1 and 3.4	T159L137 and ORCA1	OSTIA/NCEP (nudged)
U_atmos	Atmosphere	40r1	T159L137	OSTIA/NCEP (prescribed)
ERA-Interim	Atmosphere	31r2	T255L60	OSTIA/NCEP (prescribed)
U_ocean	Ocean	3.4	ORCA1	OSTIA/NCEP (nudged)
ORAS4	Ocean	3.0	ORCA1	OSTIA/NCEP (nudged)
ORAS4_nobiascrtn	Ocean	3.0	ORCA1	OSTIA/NCEP (nudged)

663 TABLE 2. Description of forecast sets described in the text. All forecasts use the same operational coupled
664 ocean-atmosphere model system (model versions 40r1 and 3.4 for IFS and NEMO respectively), but types differ
665 in the model versions and settings used for their initialisation (refer to Table 1). The sources of shock considered
666 are the three listed in Section 1.

Name	Details	Resolution	Atmos IC	Ocean IC	Sources of shock
C1	Coupled DA	T159L137/ORCA1	CERA	CERA	Baseline
U1	Uncoupled analyses, consistent models	T159L137/ORCA1	U_atmos	U_ocean	Surface imbalance
M1	Uncoupled analyses, change in models	T159L91/ORCA1	ERA-Interim	ORAS4	Surface imbalance, model version change, bias corr. removal
M2	Uncoupled analyses, change in models	T159L91/ORCA1	ERA-Interim	ORAS4.nobiascrtn	Surface imbalance, model version change
M3	Uncoupled analyses, change in atm. model	T159L91/ORCA1	ERA-Interim	U_ocean	Surface imbalance, model version change, bias corr. removal

667 **LIST OF FIGURES**

668 **Fig. 1.** The initialisation (analysis) methods used for forecast sets C1 (left), U1 (middle) and M1
669 (right). Colour coding indicates differences in model version, and elements of the analyses
670 that are not used in forecast initialisation are marked with a diagonal line. (Forecast model
671 components IFS, WAM and NEMO are the atmospheric, wave and ocean components re-
672 spectively.) 35

673 **Fig. 2.** (a) Root-mean-square difference between U_ocean SST and the SST used as forcing by
674 U_atmos, at the beginning of the forecasts, showing the imbalance present in the initialisa-
675 tion of forecasts U1; (b) the same for ORAS4 and ERA-Interim, showing one of the sources
676 of imbalance in the initialisation of forecasts M1. 36

677 **Fig. 3.** 1000 hPa temperature forecast RMSE, relative to the analysis used as the initial conditions,
678 for C1 (a), U1 (b) and M1 (c), at 12 h lead time. Land areas are masked out, as the focus is
679 on atmosphere-ocean imbalance. Contours in (b) and (c) show differences in RMSE relative
680 to C1, with blue (green) contours marking increased (decreased) RMSE in U1 and M1.
681 Contours are drawn at differences of 0.15°C in (b), and at differences of 0.5°C in (c). Only
682 differences that are significant at the 90% level, estimated using the bootstrapping method,
683 are contoured. 37

684 **Fig. 4.** Air temperature RMSE profiles averaged over the Niño3 region (150–90°W, 5°N–5°S), for
685 C1 (blue), U1 (orange) and M1 (black), evaluated against CERA, U_atmos and ERA-Interim
686 respectively, and RMSD profiles between CERA and the other two analyses (gray dashed
687 and gray dotted). Filled (open) squares mark output pressure levels where the RMSE differ-
688 ence between U1 or M1 and C1 is significant (not significant) at the 90% level, estimated
689 using the bootstrapping method. 38

690 **Fig. 5.** 1000 hPa temperature forecast RMSE averaged over the Niño3 region for C1 (blue), U1 (or-
691 ange) and M1 (black) each evaluated against their own corresponding analysis, as labelled.
692 RMSD between CERA and the other two analyses are shown for comparison (gray dashed
693 and gray dotted). Squares mark where points in the U1 and M1 series are different from
694 C1 at the 90% significance level, using confidence intervals calculated via the bootstrapping
695 method. 39

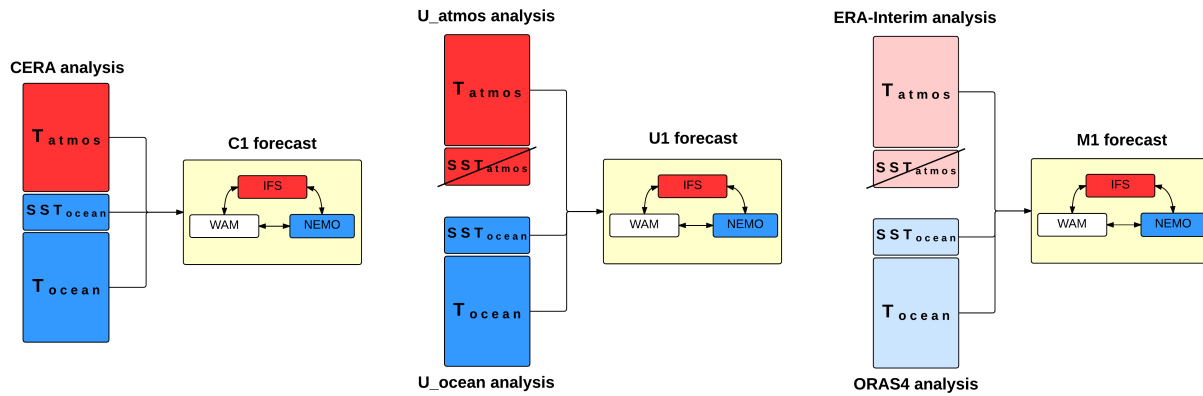
696 **Fig. 6.** SST forecast and analyses time series for the 10 start dates in Dec–Jan 2008/9, averaged over
697 the Niño3 region. Forecast series are plotted at (0, 6, 12, 18, 24) hours, and every 12 hours
698 thereafter; analysis series for CERA and U_ocean are plotted at the same frequency (U_ocean
699 features a very weak diurnal cycle), but only daily means are plotted for ORAS4 (which also
700 has a very weak diurnal cycle, not shown). Across the 10 start dates, the magnitude of the
701 drop from 0 to 6 hours in the M1 series ranges from 0.44 to 0.62°C. 40

702 **Fig. 7.** Niño3 ocean temperature (a) and upwelling velocity (b) profiles from the ocean analyses
703 U_ocean (orange) and ORAS4 (black), relative to CERA, constructed using monthly means
704 for the 6 months in 2008–2010 during which forecasts were performed. Shading shows
705 ± 1 standard deviation of the 6-month ensemble. Upwelling velocity profiles for each of the
706 three forecast periods are also shown explicitly for ORAS4 (dotted: Apr–May 2008; dashed:
707 Dec–Jan 2008/9; dash-dotted: Aug–Sep 2010). 41

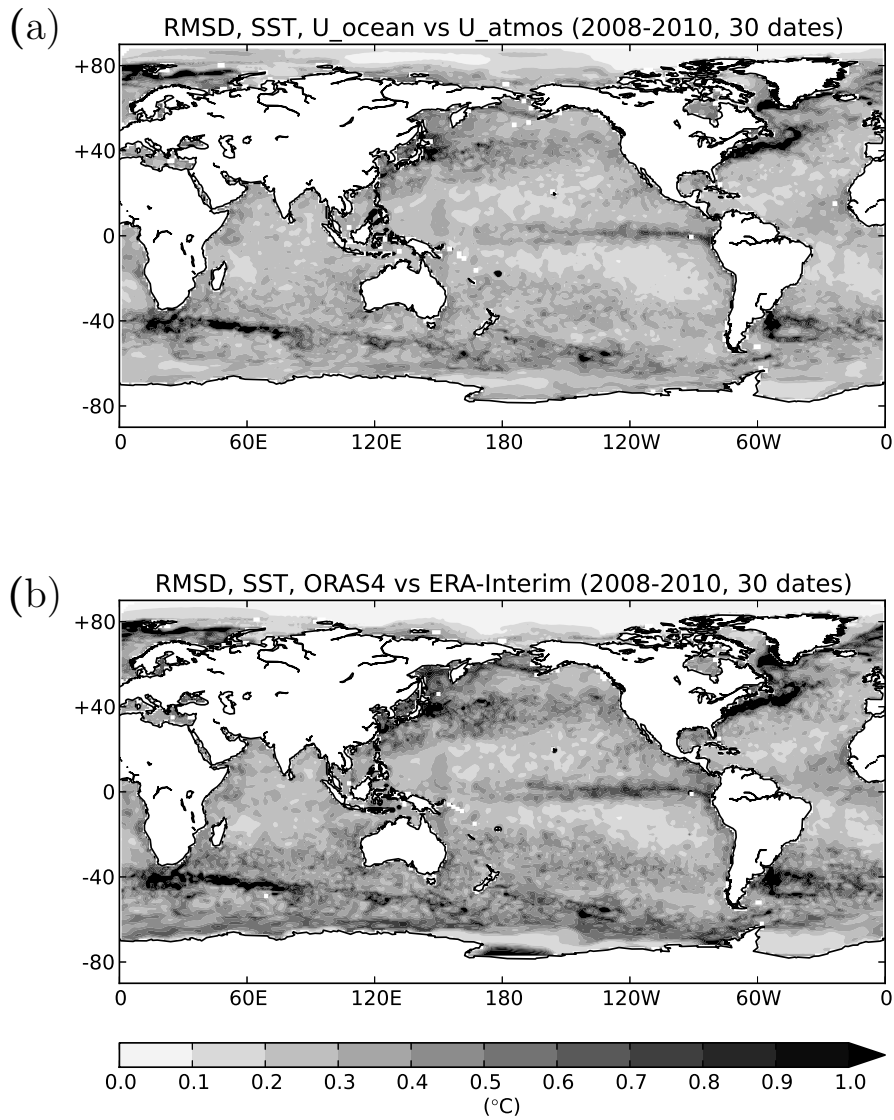
708 **Fig. 8.** Anomaly correlation coefficient for precipitation, evaluated against GPCP daily averages,
709 in the tropics (20°N–20°S, dashed) and the northern extratropics (20–60°N, solid). Squares
710 mark where points in the U1 series are different from C1 at the 90% significance level, using
711 confidence intervals calculated via the bootstrapping method. Anomalies are calculated with

712 respect to climatologies taken as the mean of the forecast period 2008–2010, which includes
713 three different seasons, so some of the skill shown here is simply due to seasonal variability. . . 42

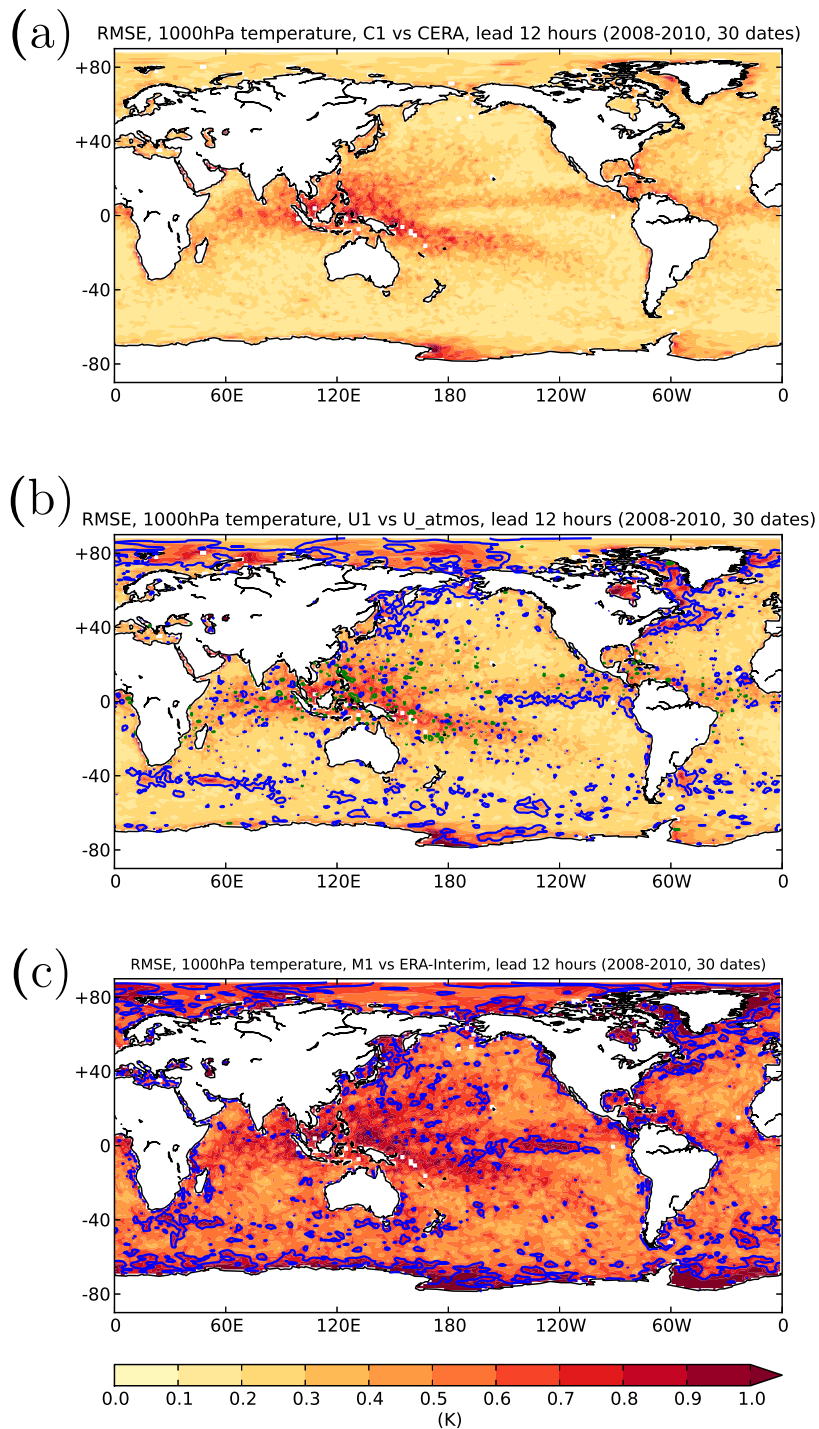
714 **Fig. 9.** (a) SST series for M1 and M2, and analyses ORAS4 and ORAS4_nobiascrtn, in the Niño3
715 region (where the largest shocks are produced in M1, M2 and M3); (b) SST series for U1,
716 M1 and M3, and analyses ORAS4 and U_ocean, again in Niño3, averaged over the ensemble
717 of 18 dates used for the M3 experiment. Forecast series are plotted at (0, 6, 12, 18, 24) hours,
718 and every 12 hours thereafter; analysis series U_ocean is plotted at the same frequency, but
719 only daily means are plotted for ORAS4 and ORAS4_nobiascrtn. 43



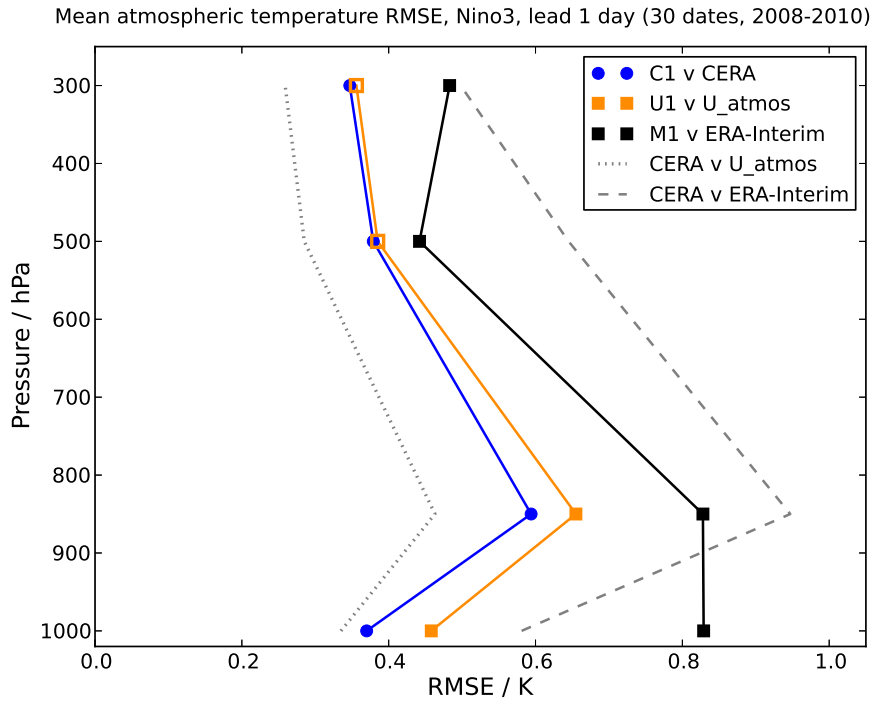
720 FIG. 1. The initialisation (analysis) methods used for forecast sets C1 (left), U1 (middle) and M1 (right).
 721 Colour coding indicates differences in model version, and elements of the analyses that are not used in forecast
 722 initialisation are marked with a diagonal line. (Forecast model components IFS, WAM and NEMO are the
 723 atmospheric, wave and ocean components respectively.)



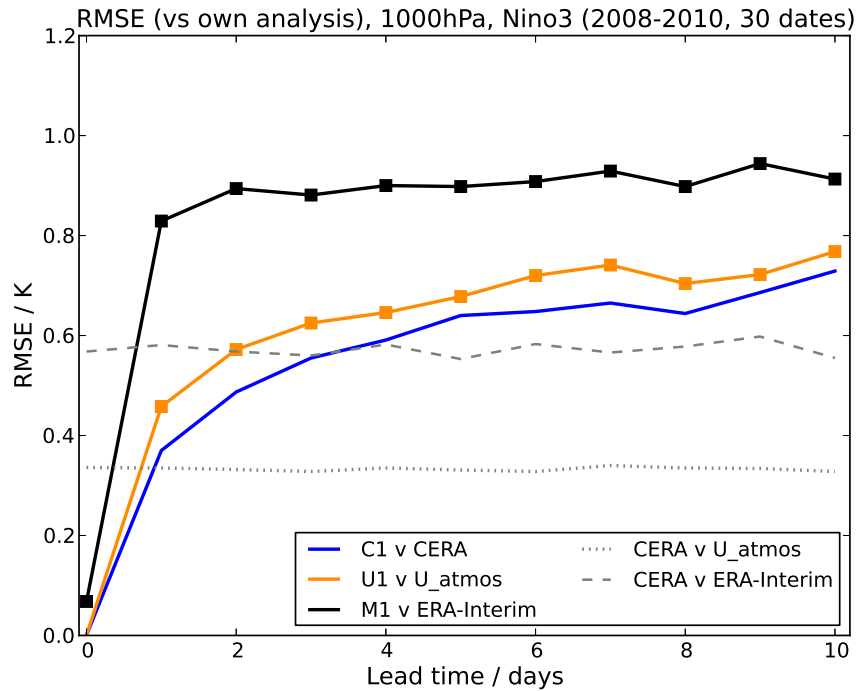
724 FIG. 2. (a) Root-mean-square difference between U_ocean SST and the SST used as forcing by U_atmos, at
 725 the beginning of the forecasts, showing the imbalance present in the initialisation of forecasts U1; (b) the same
 726 for ORAS4 and ERA-Interim, showing one of the sources of imbalance in the initialisation of forecasts M1.



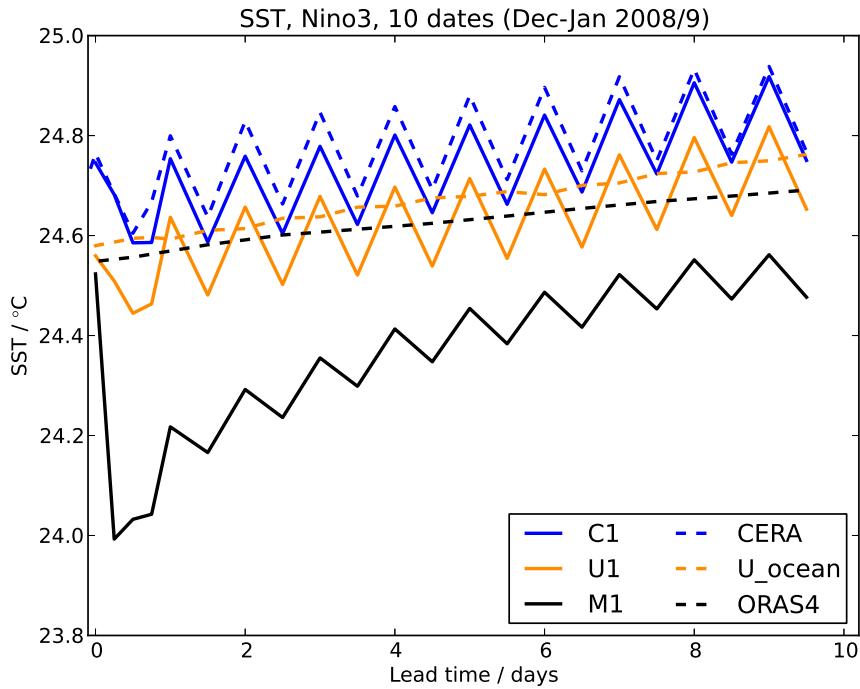
727 FIG. 3. 1000 hPa temperature forecast RMSE, relative to the analysis used as the initial conditions, for C1 (a),
 728 U1 (b) and M1 (c), at 12 h lead time. Land areas are masked out, as the focus is on atmosphere-ocean imbalance.
 729 Contours in (b) and (c) show differences in RMSE relative to C1, with blue (green) contours marking increased
 730 (decreased) RMSE in U1 and M1. Contours are drawn at differences of 0.15°C in (b), and at differences of
 731 0.5°C in (c). Only differences that are significant at the 90% level, estimated using the bootstrapping method,
 732 are contoured.



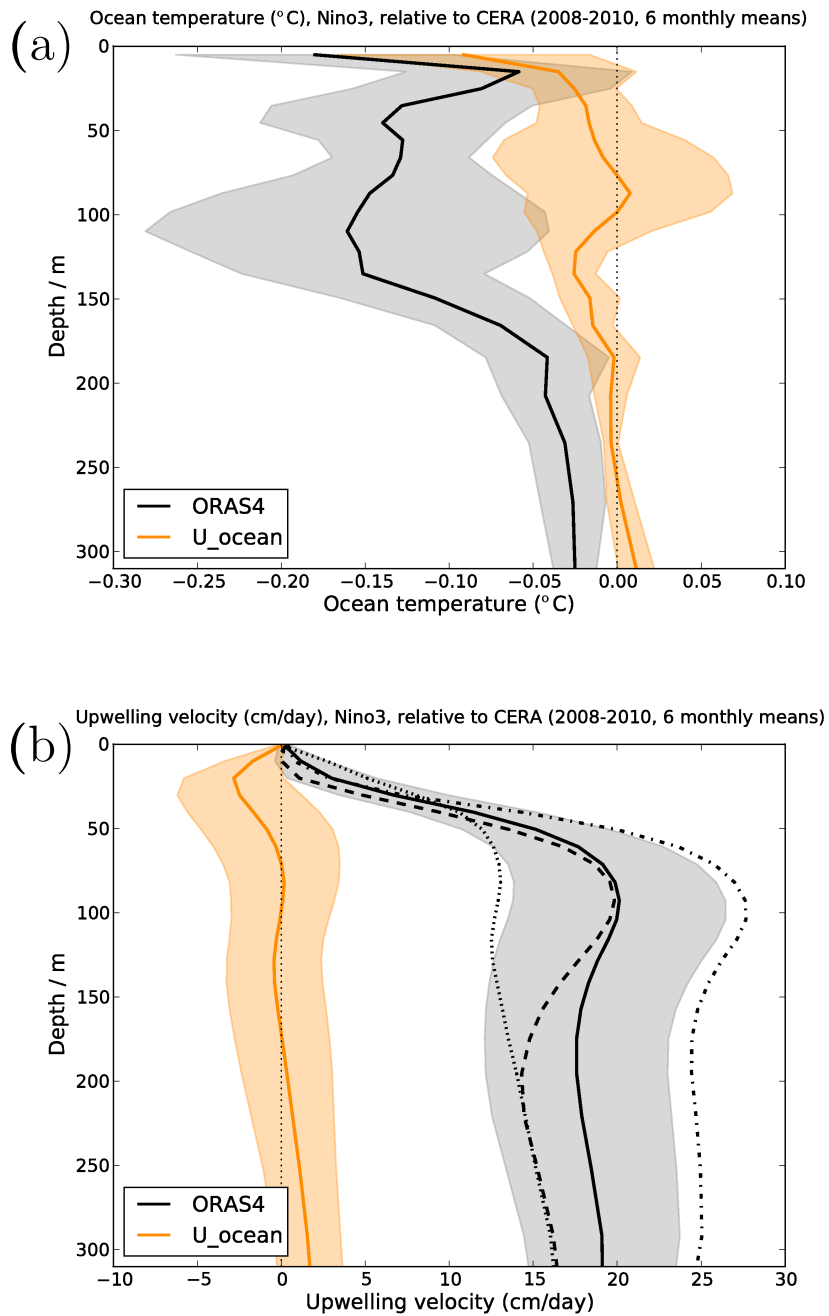
733 FIG. 4. Air temperature RMSE profiles averaged over the Niño3 region (150–90°W, 5°N–5°S), for C1 (blue),
 734 U1 (orange) and M1 (black), evaluated against CERA, U_atmos and ERA-Interim respectively, and RMSD
 735 profiles between CERA and the other two analyses (gray dashed and gray dotted). Filled (open) squares mark
 736 output pressure levels where the RMSE difference between U1 or M1 and C1 is significant (not significant) at
 737 the 90% level, estimated using the bootstrapping method.



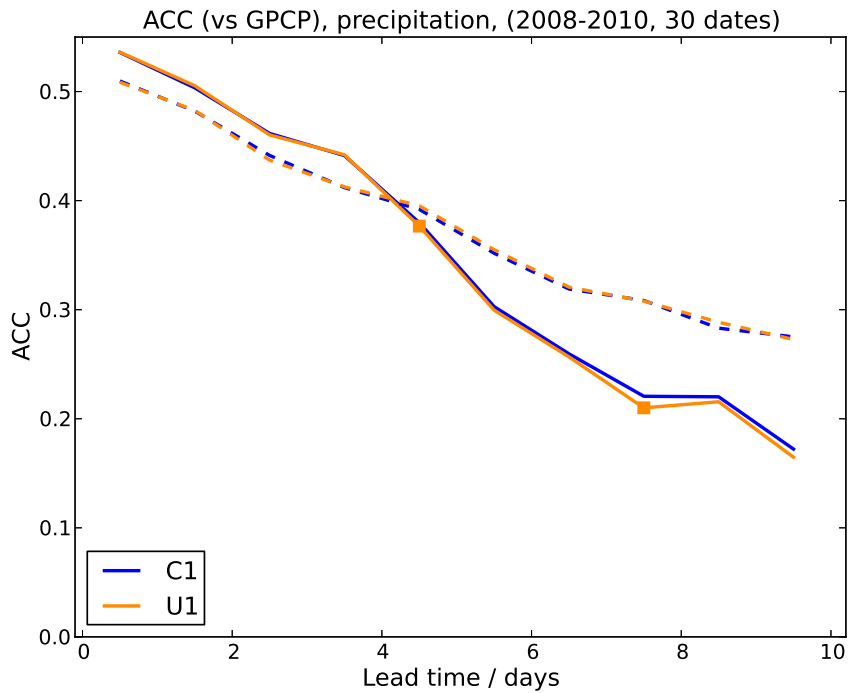
738 FIG. 5. 1000 hPa temperature forecast RMSE averaged over the Niño3 region for C1 (blue), U1 (orange) and
 739 M1 (black) each evaluated against their own corresponding analysis, as labelled. RMSD between CERA and the
 740 other two analyses are shown for comparison (gray dashed and gray dotted). Squares mark where points in the
 741 U1 and M1 series are different from C1 at the 90% significance level, using confidence intervals calculated via
 742 the bootstrapping method.



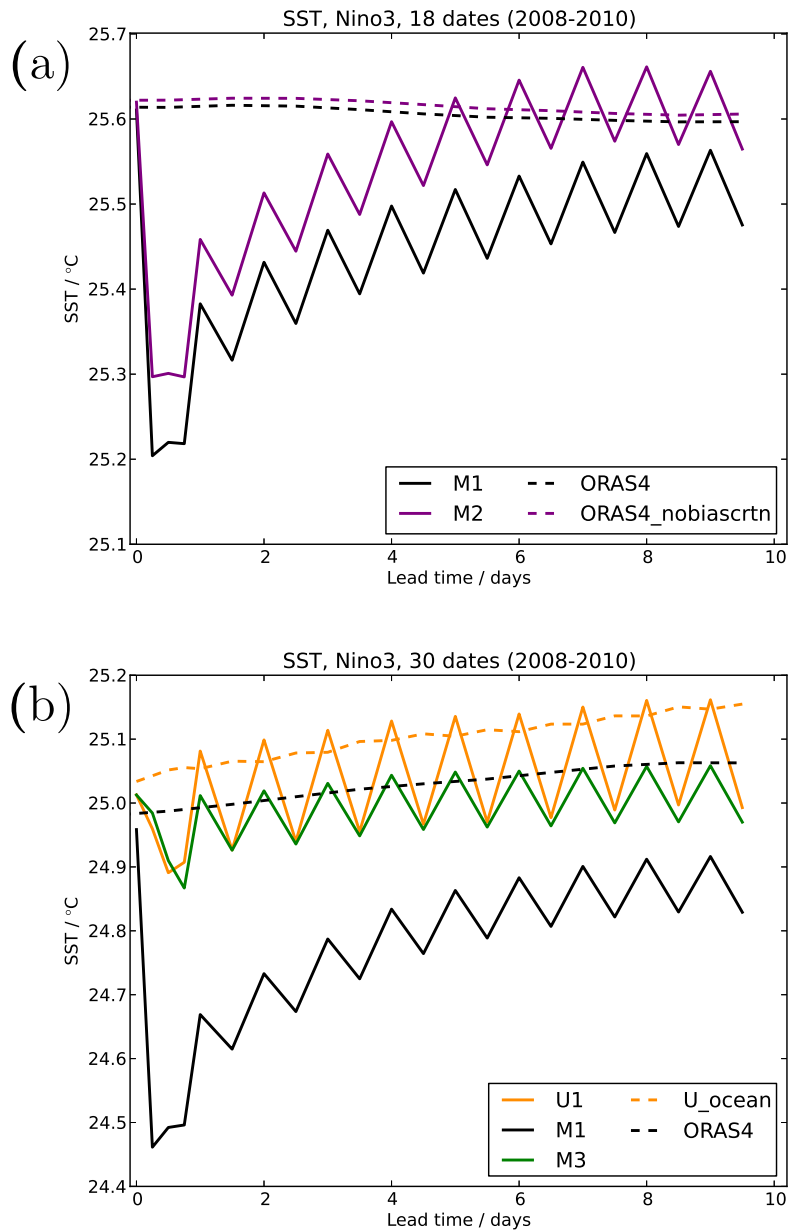
743 FIG. 6. SST forecast and analyses time series for the 10 start dates in Dec–Jan 2008/9, averaged over the
 744 Niño3 region. Forecast series are plotted at (0, 6, 12, 18, 24) hours, and every 12 hours thereafter; analysis series
 745 for CERA and U_ocean are plotted at the same frequency (U_ocean features a very weak diurnal cycle), but only
 746 daily means are plotted for ORAS4 (which also has a very weak diurnal cycle, not shown). Across the 10 start
 747 dates, the magnitude of the drop from 0 to 6 hours in the M1 series ranges from 0.44 to 0.62°C.



748 FIG. 7. Niño3 ocean temperature (a) and upwelling velocity (b) profiles from the ocean analyses U_ocean
 749 (orange) and ORAS4 (black), relative to CERA, constructed using monthly means for the 6 months in 2008–
 750 2010 during which forecasts were performed. Shading shows ± 1 standard deviation of the 6-month ensemble.
 751 Upwelling velocity profiles for each of the three forecast periods are also shown explicitly for ORAS4 (dotted:
 752 Apr–May 2008; dashed: Dec–Jan 2008/9; dash-dotted: Aug–Sep 2010).



753 FIG. 8. Anomaly correlation coefficient for precipitation, evaluated against GPCP daily averages, in the
 754 tropics (20°N – 20°S , dashed) and the northern extratropics (20 – 60°N , solid). Squares mark where points in
 755 the U1 series are different from C1 at the 90% significance level, using confidence intervals calculated via the
 756 bootstrapping method. Anomalies are calculated with respect to climatologies taken as the mean of the forecast
 757 period 2008–2010, which includes three different seasons, so some of the skill shown here is simply due to
 758 seasonal variability.



759 FIG. 9. (a) SST series for M1 and M2, and analyses ORAS4 and ORAS4.nobiascrtn, in the Niño3 region
 760 (where the largest shocks are produced in M1, M2 and M3); (b) SST series for U1, M1 and M3, and analyses
 761 ORAS4 and U_ocean, again in Niño3, averaged over the ensemble of 18 dates used for the M3 experiment.
 762 Forecast series are plotted at (0, 6, 12, 18, 24) hours, and every 12 hours thereafter; analysis series U_ocean is
 763 plotted at the same frequency, but only daily means are plotted for ORAS4 and ORAS4.nobiascrtn.